European Journal of Cell Biology 95 (2016) 195–207

Contents lists available at ScienceDirect

European Journal of Cell Biology

journal homepage: www.elsevier.com/locate/ejcb

Mutant p97 exhibits species-specific changes of its ATPase activity and compromises the UBXD9-mediated monomerisation of p97 hexamers

Ramesh Rijal[a], Khalid Arhzaouy[a], Karl-Heinz Strucksberg[a], Megan Cross[b], Andreas Hofmann[b,c], Rolf Schröder[d], Christoph S. Clemen[a,*,1], Ludwig Eichinger[a,*,1]

[a] Centre for Biochemistry, Institute of Biochemistry I, Medical Faculty, University of Cologne, 50931 Cologne, Germany
[b] Structural Chemistry Program, Eskitis Institute, Griffith University, Brisbane, Queensland 4111, Australia
[c] Faculty of Veterinary and Agricultural Sciences, The University of Melbourne, Parkville, Victoria 3030, Australia
[d] Institute of Neuropathology, University Hospital Erlangen, 91054 Erlangen, Germany

ARTICLE INFO

Article history:
Received 25 January 2016
Received in revised form 22 March 2016
Accepted 29 March 2016

Keywords:
p97/VCP/CDC48/TER/VAT ATPase
UBX domain containing protein UBXD9
UBX4/TUG/PUX/ASPL/ASPSCR1
IBMPFD
ALS
HSP
Parkinson
HMSN2
Dictyostelium discoideum
Surface plasmon resonance
Hexamer-monomer disassembly

ABSTRACT

p97 (VCP) is a homo-hexameric triple-A ATPase that exerts a plethora of cellular processes. Heterozygous missense mutations of p97 cause at least five human neurodegenerative disorders. However, the specific molecular consequences of p97 mutations are hitherto widely unknown. Our *in silico* structural models of human and *Dictyostelium* p97 showed that the disease-causing human R93C, R155H, and R155C as well as *Dictyostelium* R154C, E219K, R154C/E219K p97 mutations constitute variations in surface-exposed locations. In-gel ATPase activity measurements of p97 monomers and hexamers revealed significant mutation- and species-specific differences. While all human p97 mutations led to an increase in ATPase activity, no changes could be detected for the *Dictyostelium* R154C mutant, which is orthologous to human R155C. The E219K mutation led to an almost complete loss of activity, which was partially recuperated in the R154C/E219K double-mutant indicating p97 inter-domain communication. By means of co-immunoprecipitation experiments we identified an UBX-domain containing *Dictyostelium* protein as a novel p97 interaction partner. We categorized all UBX-domain containing *Dictyostelium* proteins and named the interaction partner UBXD9. Pull-down assays and surface plasmon resonance analyses of *Dictyostelium* UBXD9 or the human orthologue TUG/ASPL/UBXD9 demonstrated direct interactions with p97 as well as species-, mutation- and ATP-dependent differences in the binding affinities. Sucrose density gradient assays revealed that both human and *Dictyostelium* UBXD9 proteins very efficiently disassembled wild-type, but to a lesser extent mutant p97 hexamers into monomers. Our results are consistent with a scenario in which p97 point mutations lead to differences in enzymatic activities and molecular interactions, which in the long-term result in a late-onset and progressive multisystem disease.

© 2016 The Authors. Published by Elsevier GmbH. This is an open access article under the CC BY-NC-ND license (http://creativecommons.org/licenses/by-nc-nd/4.0/).

1. Introduction

p97, also known as VCP in *Homo sapiens*, TER94 *in Drosophila melanogaster*, CdcD in *Dictyostelium discoideum*, CDC48 in *Saccharomyces cerevisiae*, and VAT in *Thermoplasma acidophilum*, is a very abundant and evolutionarily highly conserved member of the triple-A (ATPase Associated with diverse cellular Activities) ATPase family (Halawani and Latterich, 2006; Madsen et al., 2009). This Mg^{2+}-dependent ATPase has a tripartite structure comprising an N-terminal CDC48 domain followed by the D1 and D2 domains that bind and hydrolyse ATP (Chou et al., 2014; DeLaBarre and Brunger, 2003). p97 assembles into a ring shaped hexameric complex of six identical subunits where the D domains form the central cylinder surrounded by the CDC48 domains (Rouiller et al., 2002; Zhang et al., 2000). The energy derived from ATP hydrolysis changes the p97 hexameric structure and is utilized to regulate cofactor binding and associated activities (Beuron et al., 2006). p97 is involved in a plethora of cellular processes such as membrane dynamics, protein quality control, cell cycle, apoptosis, and DNA damage response (Baek et al., 2013; Meyer and Weihl, 2014).

Until 2011, twenty heterozygous missense mutations had been described in human p97 with codon 155 being a mutation hot spot (Nalbandian et al., 2011). To date, the number of p97 gene mutations has markedly risen, leading to 41 different missense mutations (215th ENMC International Workshop on IBMPFD, in

* Corresponding authors.
E-mail addresses: christoph.clemen@uni-koeln.de (C.S. Clemen), ludwig.eichinger@uni-koeln.de (L. Eichinger).
[1] Co-senior authors.

http://dx.doi.org/10.1016/j.ejcb.2016.03.004
0171-9335/© 2016 The Authors. Published by Elsevier GmbH. This is an open access article under the CC BY-NC-ND license (http://creativecommons.org/licenses/by-nc-nd/4.0/).

press). Initially, it was shown that p97 mutations cause the late-onset and slowly progressive multi-system disorder IBMPFD (Inclusion Body Myopathy associated with Paget disease of bone and Fronto-temporal Dementia) (Watts et al., 2004). Meanwhile, four more neurodegenerative disorders, ALS (Amyotropic Lateral Sclerosis) (Johnson et al., 2010), Parkinson's disease (Chan et al., 2012), HSP (Hereditary Spastic Paraplegia) (de Bot et al., 2012), and Charcot-Marie-Tooth disease type 2 (HMSN2) (Gonzalez et al., 2014) have been attributed to p97 missense mutations. The exact molecular mechanisms by which p97 mutations cause these late-onset disorders remain elusive. However, an increasing number of reports showed mutation-specific effects on p97 interaction partners with functional consequences on endocytosis (Ritz et al., 2011), endoplasmic reticulum associated degradation (ERAD) of proteins (Erzurumlu et al., 2013), ATPase activity (Zhang et al., 2015), or 20S proteasome binding (Barthelme et al., 2015).

Regulation of p97 functions is mediated by many cofactors of which UBX (ubiquitin regulatory X) domain containing proteins constitute the largest subgroup (Kloppsteck et al., 2012; Schuberth and Buchberger, 2008). The UBX domain is an evolutionarily conserved 80 amino acids region that shares structural similarity with ubiquitin (Buchberger et al., 2001). Mammalian TUG (Tether containing a UBX domain for GLUT4) (Bogan et al., 2003), which is also known as ASPL (alveolar soft part sarcoma locus) (Madsen et al., 2014) or UBXD9 (Meyer and Weihl, 2014), is a member of this family and involved in insulin stimulated redistribution of the glucose transporter GLUT4 (Bogan et al., 2003) and the assembly of the Golgi complex (Orme and Bogan, 2012).

In this study, we identified an orthologous, uncharacterized *Dictyostelium* UBX domain containing protein as a novel p97 binding partner, which we accordingly named UBXD9. We assessed functional consequences of human and *Dictyostelium* p97 mutations on their ATPase activities and UBXD9 interactions. We demonstrated that disease-causing p97 mutations enhance the ATPase activity of human p97 and impede the UBXD9-mediated disassembly of human and *Dictyostelium* p97 hexamers to monomers.

2. Materials and methods

2.1. Protein sequence and domain analyses

Sequence stretches of *H. sapiens* (UniProt ID: P55072), *Mus musculus* (Q01853), *Danio rerio* (Q7ZU99), *Caenorhabditis elegans* (P54812), *D. discoideum* (DDB_G0288065), and *S. cerevisiae* (P25694) p97 were aligned using ClustalW2 (http://www.ebi.ac.uk/Tools/msa/clustalw2/). Similarly, UBXD9 protein sequences of *H. sapiens* (TUG/ASPL, Q9BZE9), *M. musculus* (TUG, Q8VBT9), *D. rerio* (TUG, Q568S9), *C. elegans* (TUG, Q17425), *D. discoideum* (UBXD9, DDB_G0279285), and *S. cerevisiae* (UBX4, P54730) were derived from UniProtKB (http://www.uniprot.org/) and dictyBase (http://www.dictybase.org/) and used for domain analysis using SMART (http://smart.embl-heidelberg.de/) and CDD (http://www.ncbi.nlm.nih.gov/Structure/cdd/cdd.shtml). Orthologous pairs of human and *Dictyostelium* UBXD proteins were determined by forward and reverse BLAST (http://blast.ncbi.nlm.nih.gov/Blast.cgi) analyses. Transmembrane domains were predicted using TMHMM (http://www.cbs.dtu.dk/services/TMHMM/). Structure-based amino acid sequence alignments were generated with SBAL (Wang et al., 2012) based on predictions of secondary structure elements with PSIPRED (Bryson et al., 2005).

2.2. Molecular modelling

Based on the crystal structure of mouse p97 (PDB entry 3cf2 Davies et al., 2008), the human p97 protein sequence, and a combination of manual modelling, geometry optimization and molecular dynamics simulation, we have constructed a full-length model of human p97 (residues 21-766 of the 806 residue protein). Using this human p97 model as a template the three-dimensional model of *D. discoideum* p97 was generated by comparative modelling with the software MODELLER (Sali and Blundell, 1993). In brief, an amino acid sequence alignment of the human and *D. discoideum* protein sequences was performed with SBAL (Wang et al., 2012) and then subjected to the routine 'automodel' in MODELLER 9v7. 100 individual models were calculated from which the model with the lowest objective function (5118.6; next lowest was 5173.1) was chosen. Subsequently, the *D. discoideum* p97 hexamer was assembled by superimposing the *D. discoideum* monomer onto each monomer of the re-constructed hexameric p97 from PDB entry 3cf2 using the software COOT (Emsley and Cowtan, 2004).

2.3. Vector construction

Vectors for the expression of wild-type and mutant human GST-p97 (Hübbers et al., 2007) and for the expression of wild-type and mutant *Dictyostelium* GST-p97 and p97-RFP (Arhzaouy et al., 2012) were previously described. For expression of human GST-UBXD9 the plasmid EX-W1107-B03 (GeneCopoeia) was used. The coding sequence of *Dictyostelium* UBXD9 was amplified by PCR from AX2 cDNA and cloned into the pGEX-6P-1 bacterial expression vector (GE Healthcare). Likewise, the UBX domain comprising amino acids 384–466 of *Dictyostelium* UBXD9 was cloned and expressed for the generation of *Dictyostelium* UBXD9-specific rabbit polyclonal antibodies (pAbs). For ectopic expression of UBXD9-GFP or GFP-UBXD9 in *Dictyostelium* cells, the UBXD9 cDNA was cloned into the *Bam*HI and *Xma*I restriction sites of pBsr-C-GFP-C1 and pBsr-N-GFP-N2 expression plasmids (Blau-Wasser et al., 2009), respectively. The expressed UBXD9 GFP-fusion proteins each contained a linker of six amino acids (GGSGGS). The inserts of all expression plasmids for human and *Dictyostelium* p97 and UBXD9 were verified by sequencing.

2.4. Dictyostelium strains and transformation

All *Dictyostelium* strains were grown at 21 °C in liquid nutrient AX2 medium (for 1 l: 14.3 g bacteriological peptone, 7.15 g yeast extract, 18 g maltose, 0.62 g $Na_2HPO_4 \times 2H_2O$, 0.49 g KH_2PO_4, pH 6.7) on 100 mm diameter plates or in shaking culture at 160 rpm (Brink et al., 1990) or on a lawn of *Klebsiella aerogenes* on SM agar plates (Williams and Newell, 1976). Expression plasmids were transformed into wild-type *Dictyostelium* AX2 cells by electroporation (Gaudet et al., 2007) and transformants were selected using 5 μg/ml BlasticidinS or 6 μg/ml G418. Stable transformants expressing GFP-UBXD9 or UBXD9-GFP were selected by fluorescence microscopy and visual inspection, and expression was verified by Western blotting using UBXD9-specific polyclonal antibodies UBX23519 or UBX23520 (see below) and anti-GFP antibodies. Similarly, strains expressing wild-type and mutant p97-RFP variants were verified by anti-RFP and anti-p97 immunoblotting. Strains expressing similar amounts of the endogenous and the corresponding fusion protein were selected for further experiments.

2.5. Purification of recombinant Dictyostelium and human p97 and UBXD9

Wild-type and mutant *Dictyostelium* GST-p97 and GST-UBXD9 fusion proteins were expressed in *Escherichia coli* XL1 Blue (New England Biolabs), wild-type and mutant human GST-p97 in *E. coli* Arctic express RIL (Stratagene), and human GST-UBXD9 in BL21 Gold (DE3) pLysS (Stratagene) cells. Cells were grown in 30 ml LB medium containing 50 μg/ml ampicillin for *E. coli* XL1 Blue,

50 μg/ml ampicillin and 20 μg/ml gentamycin for Arctic express RIL, and 50 μg/ml ampicillin and 50 μg/ml chloramphenicol for BL21 Gold (DE3) pLysS cells at 37 °C overnight. 500 ml fresh LB medium without antibiotics were inoculated with 1% overnight culture and grown at 37 °C until an OD_{600} of 0.6–0.7 followed by induction with 1 mM IPTG overnight at 21 °C for XL1 Blue and BL21 Gold (DE3) pLysS cells or at 10 °C for Arctic express RIL cells. Cells were harvested at 15,000*g* for 10 min at 4 °C, resuspended in 20 ml lysis buffer (25 mM Tris/HCl, pH 7.4, 5 mM EDTA, 0.1% Triton X-100, 10% glycerol, 150 mM NaCl, 1:50 protease inhibitor cocktail (Sigma)) and opened using an Avestin Emulsiflex C3 high pressure homogenizer (Avestin). The cell homogenates were centrifuged at 20,000*g* for 20 min at 4 °C, and 300 μl of washed glutathione sepharose 4B beads (GE Healthcare) were added to the supernatants followed by incubation under shaking for 3 h at 4 °C. GST-fusion proteins bound beads were pelleted at 500*g* for 30 s, washed 5 times with protease cleavage buffer (1x PBS with 1 mM DTT), and incubated overnight with PreScission protease (GE Healthcare) on a rotating wheel at 4 °C. Beads were centrifuged at 500*g* for 10 s and soluble proteins were collected. For quality control, aliquots of the purified proteins were fractionated by SDS-PAGE and stained by Coomassie Brilliant blue. Protein concentrations were determined by a Bradford assay.

2.6. Antibodies, immunoblotting, and protein quantitation

For generation of *Dictyostelium* UBXD9-specific polyclonal antibodies (pAbs) the GST-tag was proteolytically removed from the recombinant UBX construct and the purified UBX domain was used for immunization of rabbits (BioGenes). Resulting sera from rabbits UBX23519 and UBX23520 were diluted 1:10,000 for Western blot tests using total proteins from 2×10^5 AX2 cells. GFP was detected with mouse monoclonal antibody K3-184-2 at a 1:50 dilution (Noegel et al., 2004), RFP with a rabbit polyclonal antibody at 1:10,000 (mCherry pAb, Wiesner et al., 2010), actin with the monoclonal Act1-7 antibody at 1:50 (Simpson et al., 1984), human and *Dictyostelium* p97 with rabbit polyclonal p97_8_6841 at 1:10,000 (Arhzaouy et al., 2012), and human UBXD9 with a rabbit polyclonal antibody at 1:1,000 (#2049, Cell Signaling). Secondary antibodies used were anti-rabbit and anti-mouse IgG conjugated with peroxidase (Sigma). Detection was done by chemiluminescence in conjunction with the Fluorchem SP imaging system (Alpha Innotech); the Spot Denso tool of the AlphaEaseFC software (Alpha Innotech) was used for densitometry analyses.

2.7. Clear-native PAGE and in-gel ATPase assay

Clear-native PAGE (CN-PAGE) was performed as described (Wittig and Schägger, 2008) and used to analyse the oligomeric states of wild-type and mutant p97 proteins. Briefly, p97 proteins were expressed and purified as described above. Proteins were mixed with 3x native PAGE sample buffer (60 mM Bis-Tris, 1.5 M 6-aminocaproic acid, 60 mM NaCl, 30% glycerol) and separated on an acrylamide gel gradient (5–15% acrylamide, 500 mM 6-aminocaproic acid, pH 7.0, 50 mM Bis-Tris, pH 7.0, 0.05% APS, 0.05% TEMED) that was prepared using a peristaltic pump and a stacking gel (4% acrylamide, 500 mM 6-aminocaproic acid, pH 7.0, 50 mM Bis-Tris, pH 7.0, 0.08% APS, 0.2% TEMED). Gels were run in cathode buffer (50 mM Tricine, 15 mM Bis-Tris, 0.05% sodium deoxycholate, 0.02% *n*-dodecyl-ß-D-maltoside, pH 7.0) and anode buffer (50 mM Bis-Tris, pH 7.0) at 150 V for 4 h at 4 °C. NativeMark protein standard (Invitrogen) was used to estimate the molecular mass of the protein complexes.

The in-gel ATPase activity assay was performed as described (Zerbetto et al., 1997). Prior to the assay the amounts of wild-type and mutant p97 hexamers were estimated by Coomassie Brilliant blue stained CN-PAGE gels. Approximately equal amounts of hexamers were then separated by CN-PAGE and the gels were incubated under slight shaking at room temperature overnight in freshly prepared ATPase activity buffer 50 mM Tris/270 mM glycine solution pH 8.2, 14 mM $MgSO_4$, 8 mM ATP, 0.1% $Pb(NO_3)_2$ (note: $Pb(NO_3)_2$ is highly toxic; for optimal solubility the pH value of the final buffer is critical). The ATPase activities were visible as white bands of $Pb_3(PO_4)_2$ precipitates formed by the reaction between $Pb(NO_3)_2$ and the PO_4 produced by the ATP hydrolysis. For quantitation, gels were scanned on a black background. Next, the white precipitates were removed by overnight incubation in acid fixation solution (50% methanol, 10% acetic acid) followed by staining with Coomassie Brilliant blue and scanning for quantitation of p97 hexamer amounts.

2.8. Co-immunoprecipitation and pull-down assays

For co-immunoprecipitation experiments *Dictyostelium* cells ectopically expressing $p97^{WT}$-RFP were grown at 21 °C in 100 ml AX2 medium containing 5 μg/ml BlasticidinS. Log-phase cells ($2–4 \times 10^6$ cells/ml) were harvested by centrifugation for 5 min at 500*g* and lysed in 25 ml lysis buffer (30 mM HEPES, pH 7.5, 100 mM NaCl, 5 mM $MgCl_2$, 2 mM ATP, 1 mM DTT, 0.5% Triton X-100, 1 mM PMSF, protease inhibitor cocktail (Roche)). Homogenization was done by 20 strokes of a tightly fitting Dounce homogenizer (Wheaton). Cell homogenates were centrifuged for 20 min at 15,000*g* to spin down the cell debris and supernatants were pre-cleared with 100 μl protein A sepharose beads for 1 h at 4 °C. Another 100 μl protein A sepharose beads in PBS were incubated with 7 μl rabbit polyclonal anti-RFP serum for 2 h at 4 °C, collected by centrifugation at 500*g* for 10 s, and blocked overnight with 5% BSA in PBS on a rotating wheel at 4 °C; control beads were only incubated with BSA. The pre-cleared supernatants (7 ml) were incubated with either the antibody bound or the control beads for 90 min at 4 °C. Beads were spun down, washed two times with lysis buffer and five times with washing buffer (lysis buffer without protease inhibitor cocktail). Finally, beads were boiled for 5 min in 100 μl SDS sample buffer, and proteins were separated by 10% SDS-PAGE gels and stained with Imperial Protein Stain (Thermo-Fisher Scientific). Proteins bands were excised and proteins identified by tandem mass spectrometry (LC–MS/MS) as described (Clemen et al., 2010).

Pull-down assays were performed using the recombinant purified proteins. Wild-type or mutant *Dictyostelium* or human p97 was added to *Dictyostelium* or human GST-UBXD9 coated glutathione-beads and incubated in a final volume of 50 μl PBS supplemented with 1 mM DTT on a rotating wheel for 3 h at 4 °C. For the inverse pull-down experiments *Dictyostelium* or human UBXD9 was added to wild-type or mutant *Dictyostelium* or human GST-p97. Beads were collected by centrifugation, supernatants were kept and the beads washed five times with 150 μl PBS/DTT. 30 μl of the supernatants were mixed with 15 μl 3x SDS sample buffer, and the beads with 45 μl 1x SDS sample buffer. Supernatant and pellet fractions were analysed by Ponceau S and Coomassie Brilliant blue stains as well as immunoblotting.

2.9. Surface plasmon resonance

Surface plasmon resonance (SPR) measurements were performed using a Biacore 3000 (Biacore) system. The surface of a CM5 sensor chip (GE Healthcare) was activated by injection of a 1:1 mixture of 0.1 M *N*-hydroxysuccinimide (NHS) and 0.4 M 1-ethyl-3-(3-dimethylaminopropyl) carbodiimide hydrochloride (EDS). *Dictyostelium* or human UBXD9 was diluted to 20 μg/ml in 10 mM sodium acetate, pH 4.5, injected into one of the four flow cells and immobilized on the activated chip surface using amine-

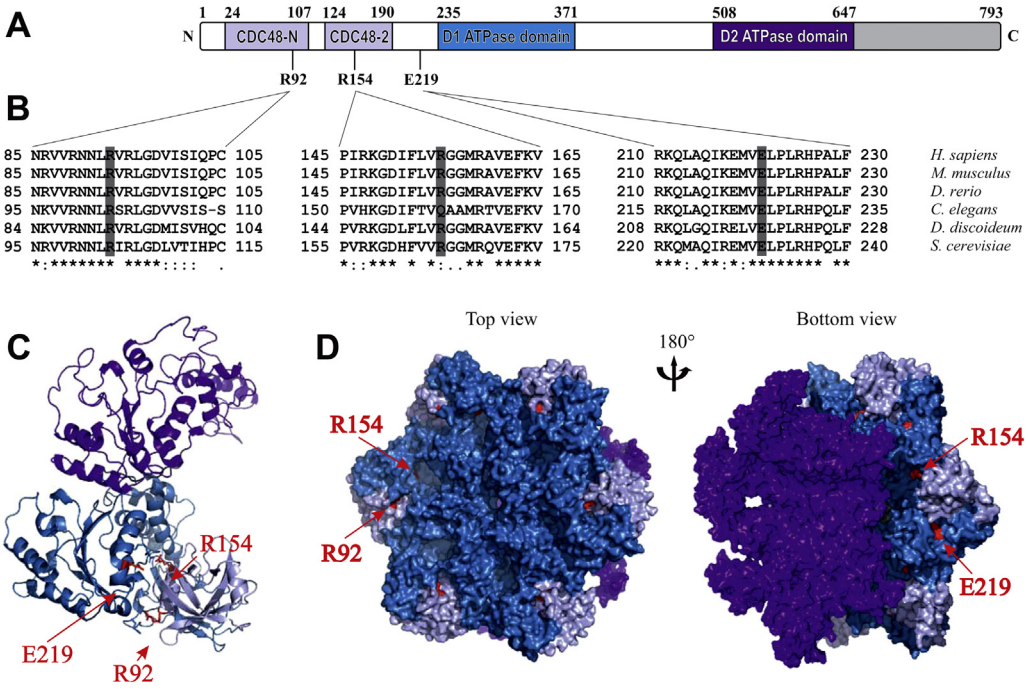

Fig. 1. Domain organization and structural information of *Dictyostelium* p97.
A. Domain organization of *Dictyostelium* p97. The N-terminal region comprising the CDC48_N and CDC48_2 domains (light blue) is followed by the D1 and D2 domains (blue and purple, respectively) and the C-terminal extension (grey). Domain structure was analysed using SMART (http://smart.embl-heidelberg.de/). B. Multiple sequence alignments of selected p97 N-terminal sequence stretches of *H. sapiens*, *M. musculus*, *D. rerio*, *C. elegans*, *D. discoideum* and *S. cerevisiae*. The highly conserved R92, R154, and E219 amino acids that were investigated in this study are highlighted. *Dictyostelium* R92 and R154 are orthologous to human R93 and R155. Multiple sequence alignments were prepared using ClustalW. Asterisks represent absolutely conserved residues; colons and periods represent conserved residues of strongly similar properties (score > 0.5) and of weakly similar properties (score ≤ 0.5 in the Gonnet PAM 250 matrix), respectively. C. Cartoon representation of a *Dictyostelium* p97 monomer. D. Surface representation of a *Dictyostelium* p97 hexamer. The N domains are coloured light blue, the D1 domains blue, the D2 domains purple, and the C-terminal extension grey. The positions of R92, R154 and E219 are indicated in red; in the hexamer, residue positions are only labelled for a single monomer. Structures were prepared with PyMOL (DeLano, 2002).

coupling. HBS-EP (0.01 M HEPES, 150 mM NaCl, 3 mM EDTA, 0.005% polysorbate 20; pH 7.4) was used as the circulating buffer for the immobilization. The remaining non-reacted ester groups were quenched with 1 M ethanolamine, pH 8.5. The amounts of immobilized *Dictyostelium* and human UBXD9 were approximately 1,500 RU. A second flow cell was activated by injection of NHS and EDC, immediately quenched with ethanolamine, and used as reference flow cell.

For kinetic studies, circulating buffer was changed to 1x PBS supplemented with 1 mM DTT and 0.005% Tween 20. Association (2 min) and dissociation (10 min) of varying concentrations of *Dictyostelium* or human wild-type or mutant p97 (5 nM to 160 nM) were monitored at 25 °C and a 30 μl/min flow rate. Base lines were achieved after the removal of bound p97 by a 90 s injection of 10 mM glycine pH 1.7 at a 30 μl/min flow rate. The response observed in the reference flow cell served as an in-line control and was subtracted for each sensorgram to correct for non-specific binding. A run of circulating buffer alone in the two flow cells was subtracted from the specific binding sensorgrams to minimize instrument noise. Kinetic parameters were analysed by globally fitting the various concentrations of p97 to the 1:1 Langmuir model using the BIAevaluation software (version 4.1).

2.10. Fluorescence microscopy

Dictyostelium cells were grown axenically on culture plates, non-adherent, dead cells were removed, and cells were detached from the surface using fresh Sørensen buffer. Coverslips of 12 mm Ø were either fixed with silica gel to the bottom of a 100 mm Ø petri dish or put in 24 well plates. 3.5×10^5 cells were allowed to adhere to each 12 mm coverslip by incubating for 30 min at room temperature. The buffer was removed and cells were fixed by addition of −20 °C cold methanol and further incubated for 5 min at −20 °C. The coverslips were washed 3 times for 5 min with 200 μl PTB buffer (1x PBS, 0.1% Triton X-100, 0.1% BSA). Fixed cells were incubated overnight at 4 °C with primary antibodies diluted in PTB buffer; UBX23519, 1:100; UBX23520, 1:100; p97_8_6841, 1:100. Then cells were washed 3 times with PTB buffer for 5 min each, and incubated with the appropriate secondary antibody, Alexa-fluor 488 goat anti-rabbit, 1:1,000 or Alexa-fluor 568 goat anti-rabbit, 1:1,000 (Invitrogen), diluted in PTB buffer. Nuclei were stained with 4′,6-diamidino-2-phenylindole (DAPI) at a final concentration of 0.5 μg/ml in PTB buffer for 1 h at room temperature in the dark. Finally, the coverslips were washed 3 times for 5 min with 200 μl PTB, 1 time with 1x PBS, 1 time with ddH_2O for 5 min, and embedded in Gelvatol. Images were acquired using a Leica DMI6000B microscope with a 100x HC Pl APO 1.4 oil immersion objective equipped with the Quorum Ångström structured illumination technique (Optigrid module) and the Leica MM-AF software (v.1.3.0).

2.11. Sucrose density gradient sedimentation assay

To analyse the oligomeric state of wild-type and mutant *Dictyostelium* and human p97 in the presence or absence of UBXD9, sucrose density gradient sedimentation was performed adapted from (Orme and Bogan, 2012). Gradients were prepared in 13.5 ml ultra-clear centrifugation tubes (Beckman Coulter) by layering 1 ml volumes of sucrose in gradient buffer (20 mM Hepes, pH 7.4, 150 mM KCl, 1 mM $MgCl_2$). The concentrations of sucrose were successively decreased from 1.1 M at the bottom to 0.3 M at the top in 0.1 M steps. Wild-type or mutant *Dictyostelium* or human p97 was incubated with and without *Dictyostelium* or human UBXD9 in equimolar ratios without ATP for 30 min prior to sedimentation. Samples were loaded onto the gradients and cen-

trifuged at 120,000*g* in a SW41 Ti (III) rotor (Beckman Coulter) for 16 h at 4 °C. Fractions of 0.5 ml were collected from the top of the gradient. From each fraction 50 μl samples were taken, mixed with 25 μl 3x SDS sample buffer, and analysed by SDS-PAGE and Coomassie Brilliant blue staining.

3. Results

3.1. Domain structure and homology model of Dictyostelium p97

The highly conserved triple-A ATPase p97 is composed of the N-terminal CDC48 domain, the two ATPase domains D1 and D2, and a non-classified C-terminal region (Fig. 1A). From the reported 41 human p97 point mutations (215th ENMC International Workshop on IBMPFD, in press), we selected R155C and R155H, the two most frequently reported p97 mutations, and R93C for further analyses. For these three mutations we previously studied the IBMPFD skeletal muscle pathology (Hübbers et al., 2007). For *Dictyostelium* p97, we included in this study the R154C mutation (Arhzaouy et al., 2012), which is orthologous to human R155C p97. Furthermore, we analysed the *Dictyostelium* R154C/E219K double-mutant p97, which was accidentally created in our p97 *in vitro* mutagenesis. For comparative analysis we generated the E219K single mutant p97, although this mutation has so far not been described to cause disease. Alignments of sequence stretches bordering the mutated residues showed that these regions are highly conserved from yeast to man (Fig. 1B).

Human and *Dictyostelium* p97 share 81% identity and 89% similarity on the amino acid sequence level and have an almost identical order and composition of secondary structure elements (Fig. S1). As no crystal structure of *Dictyostelium* p97 is available, we used the mouse p97 structure (PDB entry 3cf2 Davies et al., 2008), which possesses the most extended coverage, for the generation of full-length human and *Dictyostelium* p97 homology models. First, we used a combination of manual modelling, geometry optimization and molecular dynamics simulations to construct the human p97 model based on the mouse crystal structure and the human sequence (Genbank entry AAI10914). In a second step, the human model and the *Dictyostelium* sequence (DDB_G0288065) served to generate a structural model of *Dictyostelium* p97 (Fig. 1C). Finally, the *Dictyostelium* p97 hexamer was assembled by superimposing the obtained monomer structure onto each monomer of the mouse p97 hexamer. Our three-dimensional models of *Dictyostelium* and human p97 showed that the investigated mutated amino acids are all located on the surface of p97 and thus are accessible for interaction partners (Fig. 1D).

3.2. In-gel p97 ATPase activity measurements reveal significant mutation- and species-specific differences

We analysed and compared the ATPase activities of human and *Dictyostelium* wild-type and mutant p97 proteins. Though the ATPase activity is crucial for p97 functions, effects of mutations are still a matter of debate. This may be attributed to the methodology of a conventional ATPase assay in solution, where the results may be influenced by degradation products or contaminations from protein purification. To circumvent these problems we established an in-gel ATPase activity stain approach after clear-native polyacrylamide gel electrophoresis (CN-PAGE). We subjected recombinant human $p97^{WT}$, $p97^{R155C}$, $p97^{R155H}$, and $p97^{R93C}$ as well as *Dictyostelium* $p97^{WT}$, $p97^{R154C}$, $p97^{E219K}$, and $p97^{R154C/E219K}$ to CN-PAGE followed by the ATPase activity assay and finally Coomassie Brilliant blue stains. Notably, all missense mutations of human p97 caused a marked increase in the ATPase activity of p97 hexamers as compared to the wild-type protein.

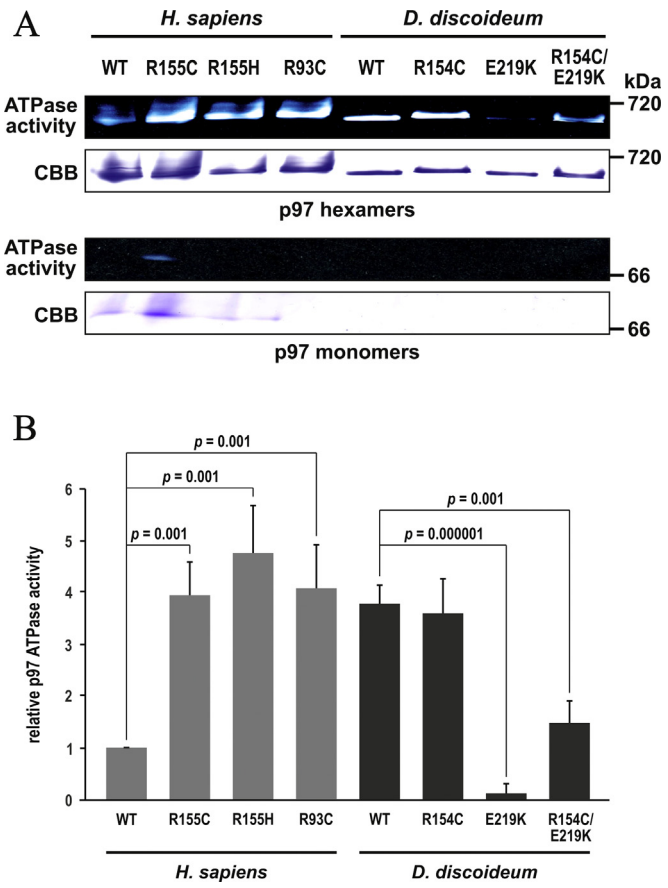

Fig. 2. In-gel ATPase activity of recombinant human and *Dictyostelium* wild-type and mutant p97 proteins.
A. Proteins were subjected to 5–15% gradient CN-PAGE. Upper panel, gel part containing p97 hexamers at approximately 600 kDa; lower panel, part from the same gel with p97 monomers at approximately 100 kDa. Upper rows, in-gel ATPase activity stain based on the formation of white precipitates of lead phosphate; lower rows, subsequent Coomassie Brilliant blue (CBB) staining. B. Quantitative analysis showing the ATPase activities of human (light grey) and *Dictyostelium* (dark grey) wild-type and mutant p97 hexamers after normalization to the protein content with human $p97^{WT}$ scaled to 1. Bars show mean values and standard deviations of 3–7 independent experiments; p-values were calculated by Student's t-test.

Moreover, we also observed weak ATPase activity at the position of $p97^{R155C}$ monomers (Fig. 2A). Quantitation and normalization by densitometry analysis of the ATPase and Coomassie Brilliant blue intensities revealed an approximately four-fold increase in ATPase activity of the human p97 mutations (Fig. 2B, grey bars). In contrast, we did not observe an increase in the ATPase activity of the orthologous *Dictyostelium* $p97^{R154C}$ mutant as compared to $p97^{WT}$. Our additional E219K mutation, although not located within the D1-domain, led to an almost complete loss of ATPase activity, which was partially recuperated in the $p97^{R154C/E219K}$ double-mutant (Fig. 2B, black bars). A comparison of the ATPase activities of human and *Dictyostelium* wild-type p97 hexamers showed that the ATPase activity of wild-type *Dictyostelium* p97 was considerably higher than that of the human orthologue. Thus, despite high structural conservation human and *Dictyostelium* p97 proteins differed significantly in mutation-induced changes as well as in their basal ATPase activities.

3.3. Dictyostelium and human UBXD9 proteins directly interact with p97

We performed co-immunoprecipitation experiments using total cell lysates from *Dictyostelium* cells ectopically expressing

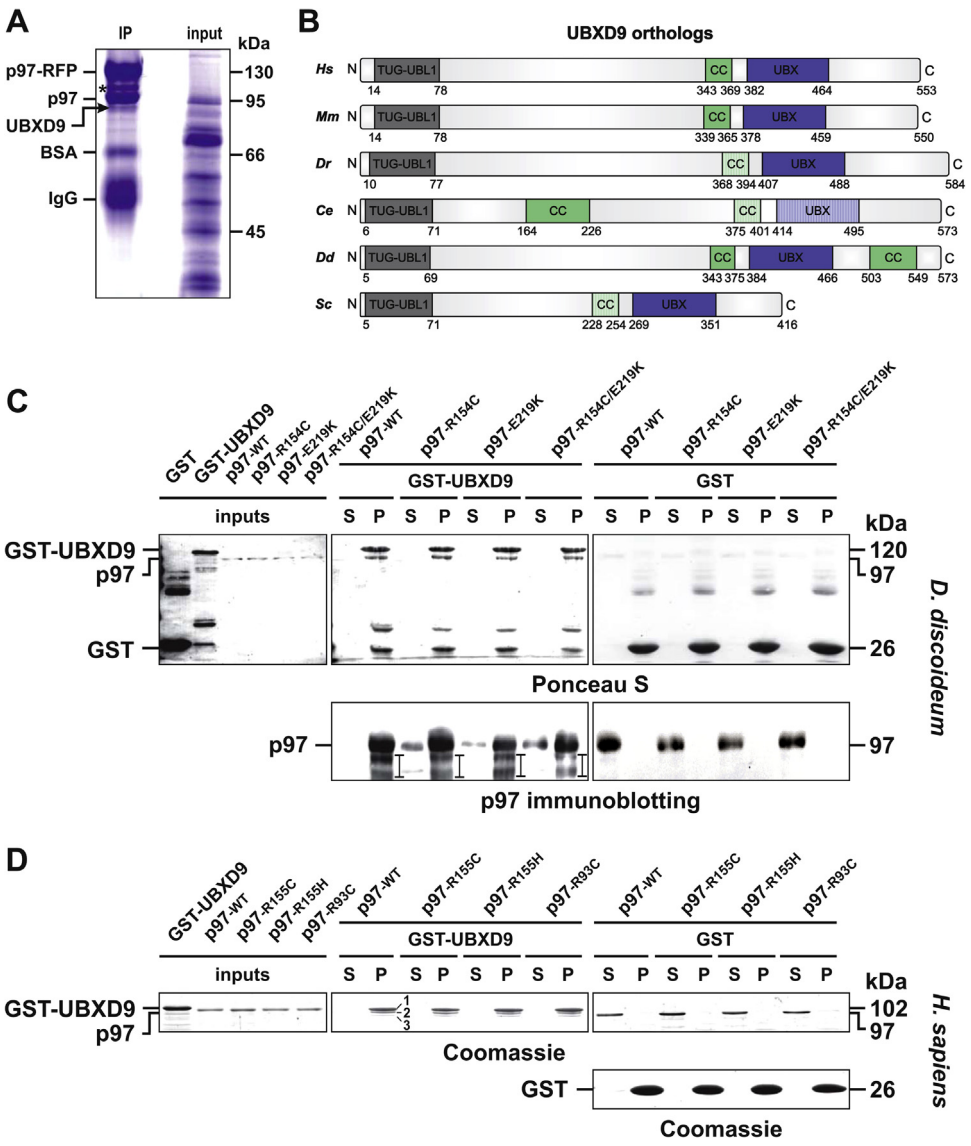

Fig. 3. *Dictyostelium* and human UBXD9 orthologues directly interact with p97.
A. For co-immunoprecipitation experiments total cell lysate from AX2/p97^{WT}-RFP cells was used (input). RFP antibodies co-precipitated p97^{WT}-RFP and endogenous p97 together with UBXD9 (IP). Protein bands were excised and subjected to mass spectrometry analyses. Asterisk, degradation product of p97^{WT}-RFP. B. Domain organization of UBXD9 orthologues from *H. sapiens (Hs), M. musculus (Mm), D. rerio (Dr), C. elegans (Ce), D. discoideum (Dd)* and *S. cerevisiae (Sc)*. The TUG-UBL1 domains are coloured dark grey, the coiled coil domains green, and the UBX domains blue. Protein domains were predicted using SMART (http://smart.embl-heidelberg.de/) and CDD (http://www.ncbi.nlm.nih.gov/Structure/cdd/cdd.shtml). Although both domain prediction programs did neither predict an UBX domain nor a correctly positioned coiled coil domain for *C. elegans* UBXD9 and no coiled coil domains for *D. rerio* UBXD9 and *S. cerevisiae* UBXD9 (UBX4), manual sequence alignments with human UBXD9 revealed the presence of these domains in all cases (hatched blue and hatched green). A further secondary structure-based alignment of the UBXD9 proteins confirmed the existence of α-helices in the predicted coiled coil domains (data not shown). Numbers indicate amino acid positions. C. Pulldown assay using recombinant *Dictyostelium* GST-UBXD9 coupled to glutathione beads or GST for control together with recombinant *Dictyostelium* non-tagged wild-type or mutant p97 (inputs). Upper panels, Ponceau S staining; lower panels, p97 immunoblotting. UBXD9 pulled down very efficiently wild-type p97 (P) with no protein visible in the supernatant (S) and, to a slightly lesser extent p97^{R154C}, p97^{E219K}, and p97$^{R154C/E219K}$. In the controls wild-type and mutant p97 was only detected in the supernatant. Distance labels indicate p97 degradation products. D. Pulldown assay using recombinant human GST-UBXD9 or GST for control coupled to glutathione beads together with recombinant human non-tagged p97^{WT}, p97^{R155C}, p97^{R155H}, and p97^{R93C} (inputs). Panels show Coomassie stained gels. GST-UBXD9 pulled down very efficiently wild-type and mutant p97 (P) with no protein visible in the supernatant (S). 1, GST-UBXD9; 2, p97; 3, degradation product of UBXD9. In the control p97 was predominantly present in the supernatant.

p97^{WT}-RFP (Arhzaouy et al., 2012). This resulted in the co-precipitation and mass spectrometry-based identification of an uncharacterized UBX domain containing (UBXD) protein (Fig. 3A). Sequence analyses showed that this protein with an apparent molecular mass of 95 kDa is one of 11 UBXD proteins in *Dictyostelium*. Similarity searches further revealed that the *Dictyostelium* protein is the orthologue of the human TUG (Tether containing UBX domain for GLUT4) protein (Bogan et al., 2003), also known as ASPL (Madsen et al., 2014) or UBXD9 (Meyer and Weihl, 2014), which is one out of 13 members of the human UBXD proteins (Meyer and Weihl, 2014). Since none of the 11 *Dictyostelium* UBXD proteins had been characterized so far, we categorized these proteins based on sequence comparisons with the 13 human UBXD proteins and found that only five of the *Dictyostelium* and human UBXD proteins were clear orthologues (Table 1). In view of inconsistent naming and consecutive numbering of UBXD proteins in e.g., human, yeast and plants, we propose a naming scheme that completes the human numbering with addition of UBXD10, 11, and 13, and extends the consecutive UBXD protein numbering with the non-orthologous *Dictyostelium* UBXD proteins 14–19.

Table 1
Categorization and proposed naming scheme of the 13 human and 11 *Dictyostelium* UBX domain containing (UBXD) proteins. The naming scheme completes the human numbering with addition of UBXD10, 11, and 13, and extends the consecutive UBXD protein numbering with the non-orthologous *Dictyostelium* UBXD proteins 14–19. Based on size, sequence similarity and domain structure five of the human and *Dictyostelium* UBXD proteins are clear orthologues.

Dictyostelium discoideum			*Homo sapiens*				homology scores		
dictyBase ID	proposed protein name	aa	protein name	UniProt ID	HUGO gene name	aa	% identity to human protein	% similarity to human protein	% coverage of Dicty protein
			UBXD1	Q9BZV1	UBXN6	441			
			UBXD2 (Erasin)	Q92575	UBXN4	508			
			UBXD3	Q96LJ8	UBXN10	280			
			UBXD4	P68543	UBXN2A	259			
			UBXD5 (Socius;COA-1)	Q5T124	UBXN11	520			
DDB_G0269774	UBXD6	264	UBXD6 (Rep-8)	O00124	UBXN8	270	28	56	30[b]
DDB_G0270358	UBXD7	503	UBXD7	O94888	UBXN7	489	28	48	97
DDB_G0280423	UBXD8	362	UBXD8	Q96CS3	FAF2	445	29	52	83
DDB_G0279285	UBXD9	573	UBXD9 (TUG;ASPL)	Q9BZE9	ASPSCR1	553	28	51	50[c]
DDB_G0293498	UBXD10	415	UBXD10[a] (p47)	Q9UNZ2	NSFL1C	370	33	52	99
			UBXD11[a] (p37)	Q14CS0	UBXN2B	331			
			UBXD12	Q9UNN5	FAF1	650			
			UBXD13[a] (SAKS1)	Q04323	UBXN1	297			
DDB_G0289369	UBXD14	420							
DDB_G0268260	UBXD15	391							
DDB_G0291259	UBXD16	543							
DDB_G0268746	UBXD17	409							
DDB_G0276057	UBXD18	540							
DDB_G0274349	UBXD19	662							

[a] Newly proposed human protein name.
[b] The human and *Dictyostelium* UBXD6 harbour in addition to the C-terminal UBX domain an N-terminal transmembrane domain.
[c] Human and *Dictyostelium* UBXD9 proteins are similar in size and have the same domain structure, see Fig. 3B.

The proposed numbering scheme has the advantage that naming of orthologues with the same number will be straightforward and allows for extension by further non-orthologous UBXD family members from other organisms. Accordingly, we named the identified *Dictyostelium* UBX domain containing protein as UBXD9 (Table 1). UBXD9 proteins contain the conserved TUG-UBL1 domain of approximately 60 amino acids at the N-terminus and an 80 amino acids UBX domain in the C-terminal part. Furthermore, our sequence analyses revealed that all members harbour in addition a coiled coil domain preceding the UBX domain (Fig. 3B).

In a next step, we first performed pull-down assays to verify the *Dictyostelium* p97–UBXD9 protein interaction and to address potential effects of point mutations in p97. We analysed the interaction of recombinant GST-UBXD9 with *Dictyostelium* $p97^{WT}$, $p97^{R154C}$, $p97^{E219K}$ and $p97^{R154C/E219K}$ (Fig. 3C). We confirmed that p97 and UBXD9 interacted directly. GST-UBXD9 completely pulled down wild-type p97 into the pellet fraction. Moreover, we found that all point mutated p97 variants also interacted, albeit not as strongly as wild-type p97 with some protein remaining in the supernatant fraction. In control experiments using GST instead of GST-UBXD9, all p97 variants exclusively remained in the supernatant. *Vice versa* we used GST-$p97^{WT}$, −$p97^{R154C}$, −$p97^{E219K}$ and −$p97^{R154C/E219K}$ to pull down non-tagged UBXD9. Here, UBXD9 interacted to a similar extent with both wild-type GST-p97 and the three GST-tagged mutant variants (Fig. S2A,B); however, the different GST-tagged p97 proteins only partially pulled down the UBXD9. Second, we investigated the interactions of human p97 with human UBXD9. In pull-down experiments with recombinant proteins using GST-UBXD9 with human $p97^{WT}$, $p97^{R155C}$, $p97^{R155H}$ and $p97^{R93C}$, we found that also human p97 and UBXD9 interacted directly (Fig. 3D). In control pull-downs, GST did not interact with p97. In the *vice versa* experiment using human GST-tagged $p97^{WT}$, $p97^{R155C}$, $p97^{R155H}$ and $p97^{R93C}$ proteins, UBXD9 was very efficiently pulled down into the pellet fraction, whereas in the control UBXD9 did not interact with GST (Fig. S2C). In conclusion, *Dictyostelium* as well as human p97 interacted directly with the UBXD9 orthologues.

3.4. Wild-type and mutant p97 exhibit differential and species-specific interaction with UBXD9

To address the binding of p97 to UBXD9 quantitatively, we performed binding assays using the surface plasmon resonance technique. Stepwise increasing concentrations of wild-type or mutant p97 were applied onto a CM5 chip coated with *Dictyostelium* or human UBXD9 (Fig. S3). Binding characteristics of the proteins in the flow cells were monitored and the dissociation constants (k_d) were calculated. For *Dictyostelium* we obtained dissociation constants for the E219K and R154C/E219K mutations that were in the same range as for wild-type p97. In contrast, $p97^{R154C}$ exhibited a two-fold increase in the k_d value in comparison to wild-type p97 (22 vs. 11 nM) (Fig. 4A, black bars). For the orthologous R155C mutation in human p97 the opposite effect was detected with an approximately two-fold decrease in the k_d value (2.9 vs. 1.6 nM). We observed no change in the k_d value of the R155H mutation, while the R93C mutation led to an approximately two-fold increase (Fig. 4B, black bars). In agreement with our pull-down assays, we also found that the interactions of human p97 variants with UBXD9 were generally much stronger, i.e., significantly lower k_d values, than the interactions between *Dictyostelium* p97 variants and UBXD9. While these assays were performed in the absence of ATP, we also conducted all binding assays in the presence of the non-hydrolysable ATP analogue AMP-PNP (adenosine 5′-(β,γ-imido)triphosphate) (Fig. 4, grey bars). For *Dictyostelium* all AMP-PNP loaded p97 variants showed higher binding affinities in comparison to the absence of ATP. Moreover, the k_d values of the point mutated p97 variants did no longer differ from wild-type p97. In contrast, AMP-PNP loading of human p97 did not change the dissociation constants for wild-type, R155C, and R155H p97, but increased the k_d value for R93C p97. These results highlighted considerable differences in the interaction properties of *Dictyostelium* and human p97 variants with UBXD9. Moreover, they revealed major influences of the p97 missense mutations R154C/R155C and R93C on the interaction with UBXD9.

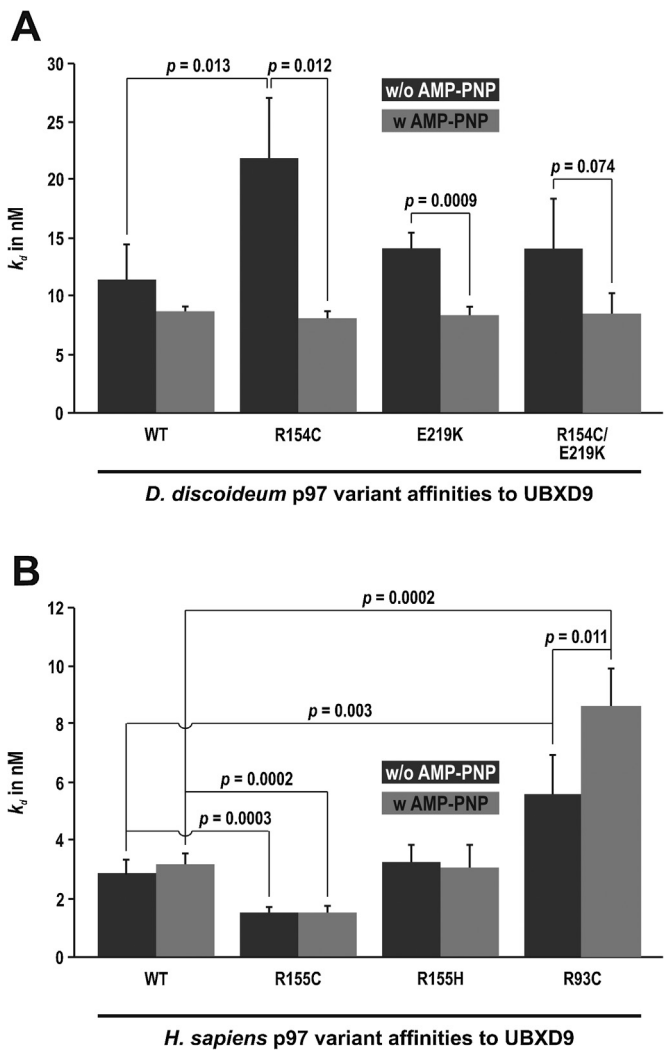

Fig. 4. Quantitation of the p97–UBXD9 interactions by surface plasmon resonance. A. Dissociation constant (k_d) values in nM of *D. discoideum* wild-type and mutant p97 binding to UBXD9 in the absence (black bars) or presence (grey bars) of the non-hydrolysable ATP analogue AMP-PNP. B. Dissociation constants of *H. sapiens* wild-type and mutant p97 binding to UBXD9 in the absence (black bars) or presence (grey bars) of AMP-PNP. Bars show mean values and standard deviations of 3 independent experiments; p-values were calculated by Student's t-test.

3.5. *Subcellular localization of* Dictyostelium *UBXD9 and wild-type and mutant p97*

Confocal imaging showed that in wild-type *Dictyostelium* cells endogenous p97, which was detected with the previously described rabbit polyclonal p97 antibody p97_8_6841 (Arhzaouy et al., 2012), was distributed throughout the cytoplasm. The distribution of endogenous UBXD9 was analysed with the newly generated rabbit polyclonal antibody UBX23520. UBXD9 was strongly visible in both the nucleus and in the cytoplasm (Fig. 5A). To further investigate the subcellular localization of p97 and UBXD9 in *Dictyostelium*, we generated AX2 strains ectopically expressing either wild-type or mutant p97 fused to RFP as well as strains expressing UBXD9 fused to GFP at its N- or C-terminus (Fig. S4). We found that over-expressed UBXD9-GFP or GFP-UBXD9 was strongly enriched in the nucleus with some additional diffuse cytoplasmic localization. The presence of the GFP-tagged UBXD9 noticeably changed the subcellular localization of the endogenous p97 and re-distributed it into the nucleus (Fig. 5B). Similarly, in cells over-expressing wild-type p97 fused to RFP part of the fusion protein re-localized to the nucleus and co-localized with endogenous UBXD9 preferentially in large patches in the nuclear periphery (Fig. 5B). To investigate the effects of the *Dictyostelium* p97 missense mutations, the localizations of RFP-tagged R154C, E219K, and R154C/E219K p97 mutants and endogenous UBXD9 were analysed. Here we found no obvious changes in the localization as compared to cells over-expressing wild-type p97-RFP (Fig. 5C).

3.6. *Normal and altered disassembly of p97 hexamers by UBXD9: a matter of wild-type and mutant p97*

To analyse molecular effects of the UBXD9–p97 interaction, both interaction partners were incubated with the respective *Dictyostelium* or human wild-type and mutant p97 proteins followed by sucrose gradient sedimentation. We found that *Dictyostelium* and human wild-type and mutant p97 hexamers were present in fractions 11–15 of higher sucrose density, while the UBXD9 proteins were enriched in fractions 3–5 of lower sucrose density (Fig. 6A,B). Incubation of either *Dictyostelium* or human UBXD9 with p97 caused a disassembly of p97 hexamers as seen by a shift of the p97 signal into fractions 5–7. Incubation of UBXD9 with p97 mutants resulted in a significantly reduced disassembly of p97 hexamers for all mutant proteins in both species (Fig. 6A,B). A quantitation of the Coomassie stained p97 signal intensities of fractions 5–7 and 11–15 showed that the disassembly of mutant p97 variants was approximately half as efficient as that of wild-type p97 (Fig. 6C). In this setting, the disassembly activity of UBXD9 is similarly affected by the orthologous R154C/R155C p97 missense mutations.

4. Discussion

The goal of the present study was the identification of novel *Dictyostelium* p97 interaction partners and the comparative analysis of *Dictyostelium* and human wild-type and mutant p97 variants with respect to their biochemical properties. In a first step, we performed *in silico* analyses to generate a complete structural model of human p97. This model was then used as a template for the calculation of a homology model for *Dictyostelium* p97. With these models, we demonstrated that the investigated mutated amino acids are located at the surface of p97, which makes them accessible for protein interactions (Fig. 1D).

In a second step, we compared the ATPase activities of human and *Dictyostelium* wild-type and mutant p97. For human p97 we chose the three disease causing mutations R155C, R155H, and R93C. For *Dictyostelium* p97 we investigated the orthologous R154C mutation and included an ATPase defective E219K mutant as well as the double mutant for these two amino acids. Previous studies had demonstrated that the second ATPase domain is crucial for p97 function (Esaki and Ogura, 2010) and exerts the major enzyme activity (Dalal et al., 2004; Song et al., 2003). More recently, a study using p97 mutants defective in ATP binding in the D1 or D2 domains revealed that also the first ATPase domain has significant ATPase activity which appeared to be regulated by ATP binding in the second domain (Chou et al., 2014). Regarding the effects of p97 disease causing mutations on its ATPase activity our literature survey revealed divergent results. For the R93C mutation, a 1.4-fold increased ATPase activity was reported (Niwa et al., 2012). While two studies on the R155H mutant reported ATPase activities similar to the wild-type enzyme (Fernandez-Saiz and Buchberger, 2010; Weihl et al., 2006), four other studies reported 1.3–3-fold increases (Manno et al., 2010; Niwa et al., 2012; Tang and Xia, 2013; Zhang et al., 2015). For the R155C mutant, two studies described 1.3–2.2-fold increases of the p97 ATPase activity (Manno et al., 2010; Niwa et al., 2012). Furthermore, one study reported a 3-

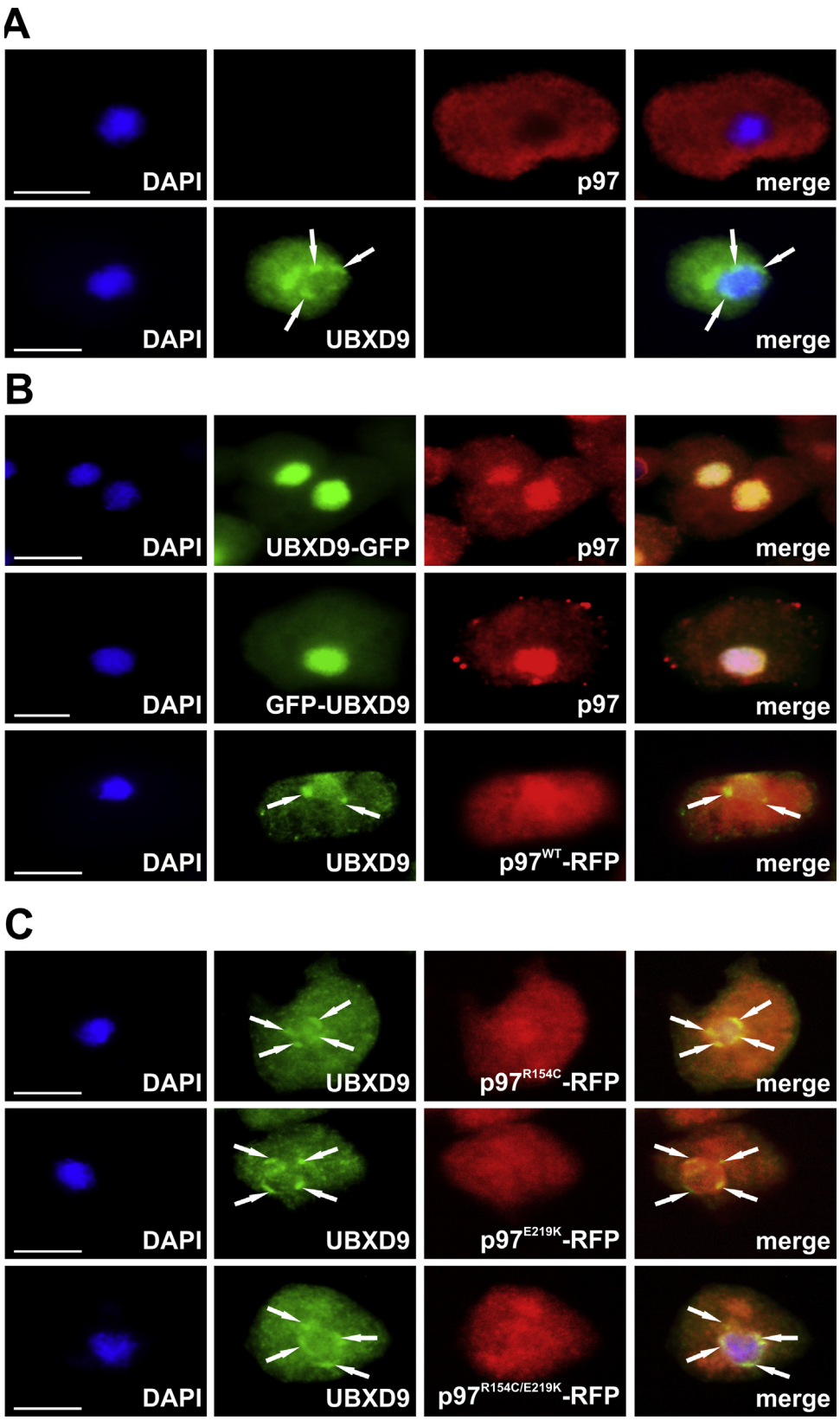

Fig. 5. Subcellular localization of *Dictyostelium* p97 and UBXD9.
A. Cytosolic localization of endogenous p97 in vegetative *Dictyostelium* wild-type AX2 cells (first row). Endogenous UBXD9 is localized to the cytosol and the nuclear periphery (second row, arrows). B. Re-localisation of the endogenous p97 into the nuclei of vegetative AX2 cells ectopically expressing UBXD9-GFP or GFP-UBXD9 (first and second rows). Ectopically expressed $p97^{WT}$-RFP was enriched in the nucleus and co-localized with endogenous UBXD9 (third row). Detection of p97 with rabbit polyclonal antibody p97_8_6841 (Arhzaouy et al., 2012). C. Localization of UBXD9 and p97 in vegetative cells ectopically expressing $p97^{R154C}$-RFP, $p97^{E219K}$-RFP, and $p97^{R154C/E219K}$-RFP. Detection of UBXD9 was done with rabbit polyclonal antibody UBX23520. Scale bars, 5 μm; single confocal planes of focus are shown.

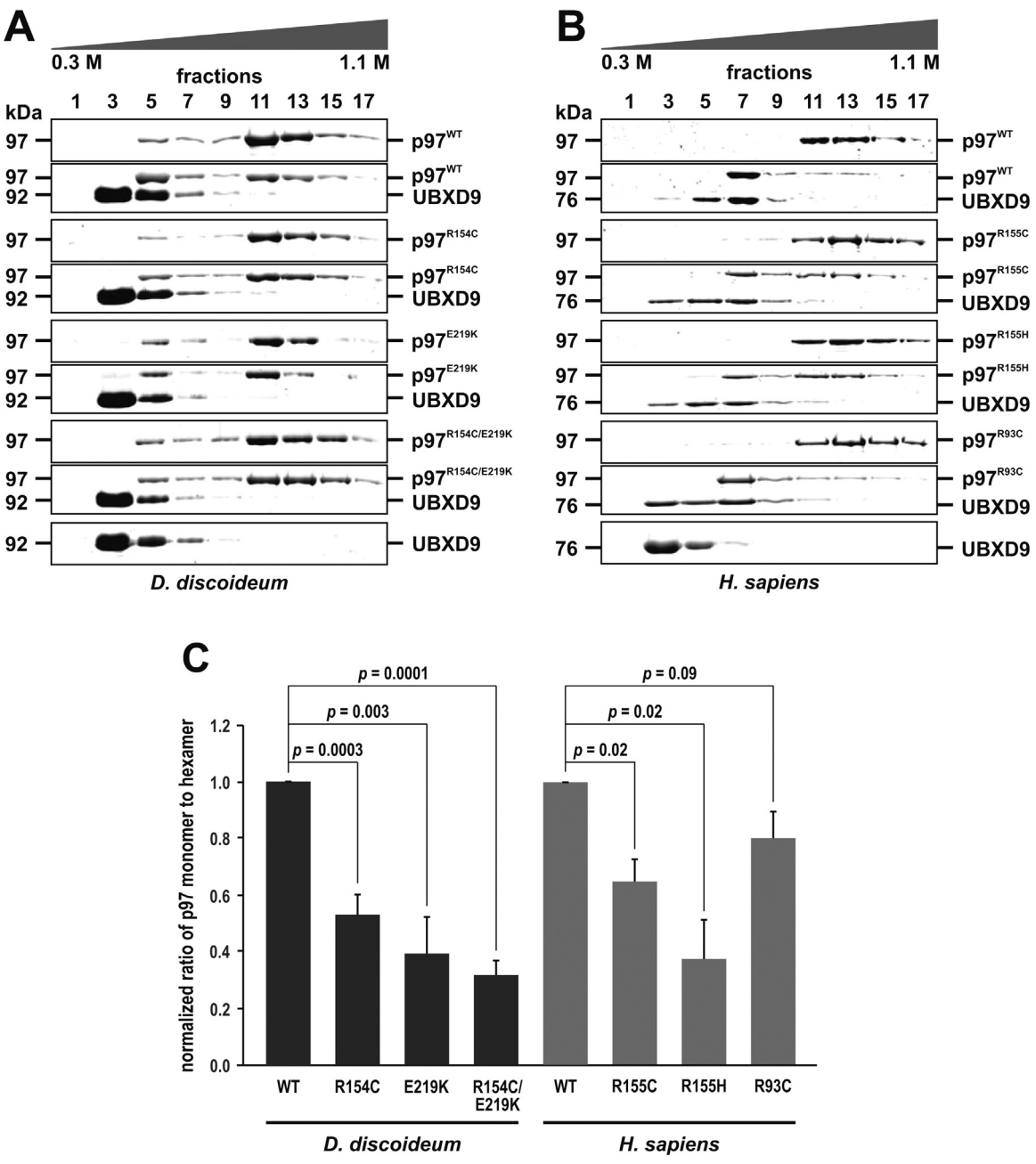

Fig. 6. Density gradient analyses of *Dictyostelium* and human wild-type and mutant p97 in the absence and presence of UBXD9.
A. Sucrose gradient centrifugation of recombinant *Dictyostelium* wild-type and mutant p97 in the absence and presence of UBXD9. Recombinant UBXD9 promoted disassembly of wild-type and mutant p97 hexamers (fractions 11–15) into monomers (fractions 5–7). Recombinant wild-type and R154C, E219K, and R154C/E219K mutant p97 proteins were pre-incubated with UBXD9 and fractionated by sucrose density gradients (0.3 M to 1.1 M). Fractions were subjected to 10% SDS-PAGE and Coomassie staining. UBXD9 alone was present in fractions 3–7. B. Sucrose gradient centrifugation of human wild-type and mutant p97 in the absence and presence of UBXD9 as described in (A). C. Quantitative analysis showing a marked decrease of p97 monomerisation for each combination of mutant p97 and UBXD9 shown in (A) and (B). Bars indicate the ratios of the signal intensities of monomeric p97 divided by the corresponding signal intensities of hexameric p97 with the wild-type ratio scaled to 1; error bars represent the standard deviation of 3 independent experiments for *Dictyostelium* and 2–3 for human; p-values were calculated by Student's t-test.

fold increased ATPase activity for the R155P p97 mutant (Halawani et al., 2009). These studies applied different types of colorimetric assays in solution for the determination of the p97 ATPase activity using either recombinant bacterial His6-p97 (Dalal et al., 2004; Fernandez-Saiz and Buchberger, 2010; Lau et al., 2015; Song et al., 2003; Weihl et al., 2006; Zhang et al., 2015), p97-His6 (Chou et al., 2014; Halawani et al., 2009; Niwa et al., 2012; Tang and Xia, 2013), myc-p97 (DeLaBarre et al., 2006), or recombinant p97-GFP purified from FreeStyle 293-F cells (Manno et al., 2010). In one case, a luminescence based ATPase assay in solution was described using recombinant His6-p97 (Chou et al., 2011).

To address putative changes of the ATPase activities, we used clear-native gels (CN-PAGE) in conjunction with an in-gel ATPase assay. This technique, which was originally described for native p97 purified from red blood cells (Harris, 1984; Peters et al., 1992; White and Ralston, 1976) and later further developed and used for mitochondrial complex V ATPase stains (Wittig et al., 2007; Zerbetto et al., 1997), has the unique advantage to stain specific protein bands and protein complexes. Thus, this approach excludes any bias

by p97 degradation products or other protein contaminations. For example, recombinant p97 from bacteria is usually contaminated with varying amounts of the chaperone and ATPase DnaK (Hsp70) (personal observation). In this context, it is noteworthy that two recent studies showed that Hsc70, another chaperone, has significant ATPase activity as compared to p97 (Kang et al., 2014; Lau et al., 2015).

Our gel-based p97 ATPase assays demonstrated that wild-type *Dictyostelium* p97 possesses four times the activity of human p97. Hexamers of mutant human R155C, R155H, and R93C p97 exhibited an approximately 4-fold higher ATPase activity than the wild-type protein. The ATPase activity, which we observed at the migrating position of $p97^{R155C}$ monomers, may either result from enzymatic active p97 monomers or from spurious amounts of p97 hexamers that may have re-assembled from monomers after CN-PAGE separation. In contrast, the *Dictyostelium* R154C p97 hexamers did not display any increase in their ATPase activity highlighting species-dependent differences. The E219K mutation of *Dictyostelium* p97, which is located close to the N-terminus of D1, nearly abolished the p97 catalytic activity, which was partially rescued by the second mutation in the R154C/E219K double-mutant (Fig. 2). The latter effect suggests an inter-domain communication involving the N- and both D-domains of p97. This hypothesis is supported by studies that demonstrated effects of the N-domain on the intrinsic ATPase activity (Fernandez-Saiz and Buchberger, 2010; Gerega et al., 2005; Halawani et al., 2009; Weihl et al., 2006) and a further report that revealed a significant ATPase activity of the p97 D1 ATPase domain (Chou et al., 2014). Based on these results, regulatory interactions between the N-, D1- and D2- domains were proposed, which are crucial for the p97 enzyme functions. This notion is further substantiated by a new study that observed substantial structural changes of the D2 ATPase domain induced by the disease-causing R155P p97 mutation (Mountassif et al., 2016).

Our search for novel p97 binding partners led to the identification of the UBL and UBX domain containing *Dictyostelium* protein UBXD9 (Table 1). UBX-domain containing proteins contribute the largest known family of p97 binding proteins (Kloppsteck et al., 2012; Meyer and Weihl, 2014; Raman et al., 2015; Schuberth and Buchberger, 2008). UBXD9 proteins constitute a subfamily, which is characterized by the additional presence of an N-terminal UBL domain (Schauber et al., 1998) and a coiled-coil domain preceding the C-terminal UBX domain (Fig. 3B). Our immunofluorescence analysis showed a cytoplasmic and nuclear localization of *Dictyostelium* UBXD9 and revealed nuclear enrichment of p97 in cells over-expressing UBXD9. A corresponding cytoplasmic and nuclear localization has previously been reported for human UBXD9 and its over-expression likewise caused accumulation of p97 in the nucleus (Orme and Bogan, 2012). We found that for mutant *Dictyostelium* p97 this UXBD9-mediated nuclear localization was not altered.

Although our *in vitro* UBXD9–p97 binding studies revealed species-specific differences in the UBXD9 interactions with *Dictyostelium* and human p97, both protein species similarly disassembled p97 hexamers. A study on the UBX-domain containing homolog PUX1 in *Arabidopsis thaliana* previously had revealed its disassembling activity on p97 hexamers (Rancour et al., 2004), and also human UBXD9 was reported to exert a p97 monomerisation activity (Orme and Bogan, 2012). We show that *Dictyostelium* R154C and the orthologous human R155C p97 mutant display a markedly decreased sensitivity to UBXD9-mediated monomerisation of p97 hexamers. The other p97 mutations of *Dictyostelium*, E219K and R154C/E219K, and of human, R93C and R155H, also caused a decreased sensitivity to UBXD9-mediated monomerisation. It seems unlikely that UBXD9 interacts with p97 at all these positions of mutant amino acids. Thus, as discussed for the ATPase activity, mutation-induced inter-domain communication changes in p97 may also be responsible for its partial resistance to monomerisation. Since both the UBL (Schauber et al., 1998; Su and Lau, 2009) and UBX (Schuberth and Buchberger, 2008) domain containing proteins are involved in the protein quality control systems, it is tempting to speculate that changes in the hexamer-monomer equilibrium of missense mutated p97 contribute to the p97 disease pathology.

Irrespective of a very high degree of p97 sequence conservation, our work highlights essential differences in the biochemical properties of *Dictyostelium* and human p97 orthologues. Thus, functional data of non-human p97 do not necessarily mirror the human situation and should be interpreted with caution. We demonstrate that human disease-causing p97 point mutations result in an increased ATPase activity. Moreover, they interfere with the UBXD9-mediated p97 hexamer-monomer equilibrium. As p97 and UBXD9 only co-localize to a limited extent, UBXD9 may locally regulate the function of p97. Further studies have to address the question whether the late-onset p97 human disease pathology is related to an increased ATPase activity and/or altered UBXD9 protein interactions.

Conflict of interests

The authors declare that they have no conflicts of interest with the contents of this article.

Contributors

RR, KA, and KHS designed and performed experiments and analysed data. CSC and LE designed experiments and analysed data. RS, CSC, and LE reviewed all data. MC and AH performed secondary structure predictions and the molecular modelling. RR drafted the manuscript and figures. CSC and LE prepared the final version of manuscript and figures. All authors approved the final version of the manuscript.

Acknowledgements

We thank Dr. Jan Faix, Medical School Hannover, Germany, for kindly providing the RFP rabbit polyclonal antibody. Grant support by the German Research Foundation (DFG) within the framework of the multi-location research group FOR1228 (grants CL 381/3-2 to CSC, EI 399/7-2 to LE, and SCHR 562/9-2 to RS), the Australian Research Council (ARC) (grant LE120100071 to AH), Equity Trustees PhD Scholarship (to MC), and by Köln Fortune (to CSC and LE) is gratefully acknowledged.

Appendix A. Supplementary data

Supplementary data associated with this article can be found, in the online version, at http://dx.doi.org/10.1016/j.ejcb.2016.03.004.

References

215th ENMC International Workshop on IBMPFD, Neuromuscul. Disord. Nov 13–15, 2015, Heemskerk, The Netherlands, in press.

Arhzaouy, K., Strucksberg, K.H., Tung, S.M., Tangavelou, K., Stumpf, M., Faix, J., Schroder, R., Clemen, C.S., Eichinger, L., 2012. Heteromeric p97/p97(R155C) complexes induce dominant negative changes in wild-type and autophagy 9-deficient *Dictyostelium* strains. PLoS One 7, e46879.

Baek, G.H., Cheng, H., Choe, V., Bao, X., Shao, J., Luo, S., Rao, H., 2013. Cdc48: a swiss army knife of cell biology. J. Amino Acids 2013, 183421.

Barthelme, D., Jauregui, R., Sauer, R.T., 2015. An ALS disease mutation in Cdc48/p97 impairs 20S proteasome binding and proteolytic communication. Protein Sci. 24, 1521–1527.

Beuron, F., Dreveny, I., Yuan, X., Pye, V.E., McKeown, C., Briggs, L.C., Cliff, M.J., Kaneko, Y., Wallis, R., Isaacson, R.L., Ladbury, J.E., Matthews, S.J., Kondo, H., Zhang, X., Freemont, P.S., 2006. Conformational changes in the AAA ATPase p97-p47 adaptor complex. EMBO J. 25, 1967–1976.

Blau-Wasser, R., Euteneuer, U., Xiong, H., Gassen, B., Schleicher, M., Noegel, A.A., 2009. CP250, a novel acidic coiled-coil protein of the Dictyostelium centrosome, affects growth, chemotaxis, and the nuclear envelope. Mol. Biol. Cell 20, 4348–4361.

Bogan, J.S., Hendon, N., McKee, A.E., Tsao, T.S., Lodish, H.F., 2003. Functional cloning of TUG as a regulator of GLUT4 glucose transporter trafficking. Nature 425, 727–733.

Brink, M., Gerisch, G., Isenberg, G., Noegel, A.A., Segall, J.E., Wallraff, E., Schleicher, M., 1990. A Dictyostelium mutant lacking an F-actin cross-linking protein, the 120-kD gelation factor. J. Cell Biol. 111, 1477–1489.

Bryson, K., McGuffin, L.J., Marsden, R.L., Ward, J.J., Sodhi, J.S., Jones, D.T., 2005. Protein structure prediction servers at University College London. Nucleic Acids Res. 33, W36–W38.

Buchberger, A., Howard, M.J., Proctor, M., Bycroft, M., 2001. The UBX domain: a widespread ubiquitin-like module. J. Mol. Biol. 307, 17–24.

Chan, N., Le, C., Shieh, P., Mozaffar, T., Khare, M., Bronstein, J., Kimonis, V., 2012. Valosin-containing protein mutation and Parkinson's disease. Parkinsonism Relat. Disord. 18, 107–109.

Chou, T.F., Brown, S.J., Minond, D., Nordin, B.E., Li, K., Jones, A.C., Chase, P., Porubsky, P.R., Stoltz, B.M., Schoenen, F.J., Patricelli, M.P., Hodder, P., Rosen, H., Deshaies, R.J., 2011. Reversible inhibitor of p97 DBeQ, impairs both ubiquitin-dependent and autophagic protein clearance pathways. Proc. Natl. Acad. Sci. U. S. A. 108, 4834–4839.

Chou, T.F., Bulfer, S.L., Weihl, C.C., Li, K., Lis, L.G., Walters, M.A., Schoenen, F.J., Lin, H.J., Deshaies, R.J., Arkin, M.R., 2014. Specific inhibition of p97/VCP ATPase and kinetic analysis demonstrate interaction between D1 and D2 ATPase domains. J. Mol. Biol. 426, 2886–2899.

Clemen, C.S., Tangavelou, K., Strucksberg, K.H., Just, S., Gaertner, L., Regus-Leidig, H., Stumpf, M., Reimann, J., Coras, R., Morgan, R.O., Fernandez, M.P., Hofmann, A., Muller, S., Schoser, B., Hanisch, F.G., Rottbauer, W., Blumcke, I., von Horsten, S., Eichinger, L., Schröder, R., 2010. Strumpellin is a novel valosin-containing protein binding partner linking hereditary spastic paraplegia to protein aggregation diseases. Brain 133, 2920–2941.

Dalal, S., Rosser, M.F., Cyr, D.M., Hanson, P.I., 2004. Distinct roles for the AAA ATPases NSF and p97 in the secretory pathway. Mol. Biol. Cell 15, 637–648.

Davies, J.M., Brunger, A.T., Weis, W.I., 2008. Improved structures of full-length p97, an AAA ATPase: implications for mechanisms of nucleotide-dependent conformational change. Structure 16, 715–726.

de Bot, S.T., Schelhaas, H.J., Kamsteeg, E.J., van de Warrenburg, B.P., 2012. Hereditary spastic paraplegia caused by a mutation in the VCP gene. Brain 135, e223.

DeLaBarre, B., Brunger, A.T., 2003. Complete structure of p97/valosin-containing protein reveals communication between nucleotide domains. Nat. Struct. Biol. 10, 856–863.

DeLaBarre, B., Christianson, J.C., Kopito, R.R., Brunger, A.T., 2006. Central pore residues mediate the p97/VCP activity required for ERAD. Mol. Cell 22, 451–462.

DeLano, W.L., 2002. The PyMOL Molecular Graphics System. http://www.pymol.org.

Emsley, P., Cowtan, K., 2004. Coot: model-building tools for molecular graphics. Acta Crystallogr. D Biol. Crystallogr. 60, 2126–2132.

Erzurumlu, Y., Kose, F.A., Gozen, O., Gozuacik, D., Toth, E.A., Ballar, P., 2013. A unique IBMPFD-related P97/VCP mutation with differential binding pattern and subcellular localization. Int. J. Biochem. Cell Biol. 45, 773–782.

Esaki, M., Ogura, T., 2010. ATP-bound form of the D1 AAA domain inhibits an essential function of Cdc48p/p97. Biochem. Cell Biol. 88, 109–117.

Fernandez-Saiz, V., Buchberger, A., 2010. Imbalances in p97 co-factor interactions in human proteinopathy. EMBO Rep. 11, 479–485.

Gaudet, P., Pilcher, K.E., Fey, P., Chisholm, R.L., 2007. Transformation of *Dictyostelium discoideum* with plasmid DNA. Nat. Protoc. 2, 1317–1324.

Gerega, A., Rockel, B., Peters, J., Tamura, T., Baumeister, W., Zwickl, P., 2005. VAT, the thermoplasma homolog of mammalian p97/VCP, is an N domain-regulated protein unfoldase. J. Biol. Chem. 280, 42856–42862.

Gonzalez, M.A., Feely, S.M., Speziani, F., Strickland, A.V., Danzi, M., Bacon, C., Lee, Y., Chou, T.F., Blanton, S.H., Weihl, C.C., Zuchner, S., Shy, M.E., 2014. A novel mutation in VCP causes charcot-marie-tooth type 2 disease. Brain 137, 2897–2902.

Hübbers, C.U., Clemen, C.S., Kesper, K., Boddrich, A., Hofmann, A., Kamarainen, O., Tolksdorf, K., Stumpf, M., Reichelt, J., Roth, U., Krause, S., Watts, G., Kimonis, V., Wattjes, M.P., Reimann, J., Thal, D.R., Biermann, K., Evert, B.O., Lochmuller, H., Wanker, E.E., Schoser, B.G., Noegel, A.A., Schröder, R., 2007. Pathological consequences of VCP mutations on human striated muscle. Brain 130, 381–393.

Halawani, D., Latterich, M., 2006. p97: the cell's molecular purgatory? Mol. Cell 22, 713–717.

Halawani, D., LeBlanc, A.C., Rouiller, I., Michnick, S.W., Servant, M.J., Latterich, M., 2009. Hereditary inclusion body myopathy-linked p97/VCP mutations in the NH2 domain and the D1 ring modulate p97/VCP ATPase activity and D2 ring conformation. Mol. Cell. Biol. 29, 4484–4494.

Harris, J.R., 1984. Biochemical and ultrastructural characterization of a high molecular weight soluble Mg2+ −ATPase from human erythrocytes. J. Mol. Biol. 174, 705–721.

Johnson, J.O., Mandrioli, J., Benatar, M., Abramzon, Y., Van Deerlin, V.M., Trojanowski, J.Q., Gibbs, J.R., Brunetti, M., Gronka, S., Wuu, J., Ding, J., McCluskey, L., Martinez-Lage, M., Falcone, D., Hernandez, D.G., Arepalli, S., Chong, S., Schymick, J.C., Rothstein, J., Landi, F., Wang, Y.D., Calvo, A., Mora, G., Sabatelli, M., Monsurro, M.R., Battistini, S., Salvi, F., Spataro, R., Sola, P., Borghero, G., Galassi, G., Scholz, S.W., Taylor, J.P., Restagno, G., Chio, A., Traynor, B.J., 2010. Exome sequencing reveals VCP mutations as a cause of familial ALS. Neuron 68, 857–864.

Kang, M.J., Wu, T., Wijeratne, E.M., Lau, E.C., Mason, D.J., Mesa, C., Tillotson, J., Zhang, D.D., Gunatilaka, A.A., La Clair, J.J., Chapman, E., 2014. Functional chromatography reveals three natural products that target the same protein with distinct mechanisms of action. ChemBioChem 15, 2125–2131.

Kloppsteck, P., Ewens, C.A., Forster, A., Zhang, X., Freemont, P.S., 2012. Regulation of p97 in the ubiquitin-proteasome system by the UBX protein-family. Biochim. Biophys. Acta 1823, 125–129.

Lau, E.C., Mason, D.J., Eichhorst, N., Engelder, P., Mesa, C., Kithsiri Wijeratne, E.M., Gunaherath, G.M., Gunatilaka, A.A., La Clair, J.J., Chapman, E., 2015. Functional chromatographic technique for natural product isolation. Org. Biomol. Chem. 13, 2255–2259.

Madsen, L., Seeger, M., Semple, C.A., Hartmann-Petersen, R., 2009. New ATPase regulators–p97 goes to the PUB. Int. J. Biochem. Cell Biol. 41, 2380–2388.

Madsen, L., Molbaek, K., Larsen, I.B., Nielsen, S.V., Poulsen, E.G., Walmod, P.S., Hofmann, K., Seeger, M., Chien, C.Y., Chen, R.H., Kriegenburg, F., Hartmann-Petersen, R., 2014. Human ASPL/TUG interacts with p97 and complements the proteasome mislocalization of a yeast ubx4 mutant, but not the ER-associated degradation defect. BMC Cell Biol. 15, 31.

Manno, A., Noguchi, M., Fukushi, J., Motohashi, Y., Kakizuka, A., 2010. Enhanced ATPase activities as a primary defect of mutant valosin-containing proteins that cause inclusion body myopathy associated with Paget disease of bone and frontotemporal dementia. Genes Cells 15, 911–922.

Meyer, H., Weihl, C.C., 2014. The VCP/p97 system at a glance: connecting cellular function to disease pathogenesis. J. Cell Sci. 127, 3877–3883.

Mountassif, D., Fabre, L., Zaid, Y., Halawani, D., Rouiller, I., 2016. Cryo-EM of the pathogenic VCP variant R155P reveals long-range conformational changes in the D2 ATPase ring. Biochem. Biophys. Res. Commun. 201 (468), 636–641.

Nalbandian, A., Donkervoort, S., Dec, E., Badadani, M., Katheria, V., Rana, P., Nguyen, C., Mukherjee, J., Caiozzo, V., Martin, B., Watts, G.D., Vesa, J., Smith, C., Kimonis, V.E., 2011. The multiple faces of valosin-containing protein-associated diseases: inclusion body myopathy with Paget's disease of bone, frontotemporal dementia, and amyotrophic lateral sclerosis. J. Mol. Neurosci. 45, 522–531.

Niwa, H., Ewens, C.A., Tsang, C., Yeung, H.O., Zhang, X., Freemont, P.S., 2012. The role of the N-domain in the ATPase activity of the mammalian AAA ATPase p97/VCP. J. Biol. Chem. 287, 8561–8570.

Noegel, A.A., Blau-Wasser, R., Sultana, H., Muller, R., Israel, L., Schleicher, M., Patel, H., Weijer, C.J., 2004. The cyclase-associated protein CAP as regulator of cell polarity and cAMP signaling in *Dictyostelium*. Mol. Biol. Cell 15, 934–945.

Orme, C.M., Bogan, J.S., 2012. The ubiquitin regulatory X (UBX) domain-containing protein TUG regulates the p97 ATPase and resides at the endoplasmic reticulum-golgi intermediate compartment. J. Biol. Chem. 287, 6679–6692.

Peters, J.M., Harris, J.R., Lustig, A., Muller, S., Engel, A., Volker, S., Franke, W.W., 1992. Ubiquitous soluble Mg(2+)-ATPase complex. A structural study. J. Mol. Biol. 223, 557–571.

Raman, M., Sergeev, M., Garnaas, M., Lydeard, J.R., Huttlin, E.L., Goessling, W., Shah, J.V., Harper, J.W., 2015. Systematic proteomics of the VCP-UBXD adaptor network identifies a role for UBXN10 in regulating ciliogenesis. Nat. Cell Biol. 17, 1356–1369.

Rancour, D.M., Park, S., Knight, S.D., Bednarek, S.Y., 2004. Plant UBX domain-containing protein 1, PUX1, regulates the oligomeric structure and activity of arabidopsis CDC48. J. Biol. Chem. 279, 54264–54274.

Ritz, D., Vuk, M., Kirchner, P., Bug, M., Schutz, S., Hayer, A., Bremer, S., Lusk, C., Baloh, R.H., Lee, H., Glatter, T., Gstaiger, M., Aebersold, R., Weihl, C.C., Meyer, H., 2011. Endolysosomal sorting of ubiquitylated caveolin-1 is regulated by VCP and UBXD1 and impaired by VCP disease mutations. Nat. Cell Biol. 13, 1116–1123.

Rouiller, I., DeLaBarre, B., May, A.P., Weis, W.I., Brunger, A.T., Milligan, R.A., Wilson-Kubalek, E.M., 2002. Conformational changes of the multifunction p97 AAA ATPase during its ATPase cycle. Nat. Struct. Biol. 9, 950–957.

Sali, A., Blundell, T.L., 1993. Comparative protein modelling by satisfaction of spatial restraints. J. Mol. Biol. 234, 779–815.

Schauber, C., Chen, L., Tongaonkar, P., Vega, I., Lambertson, D., Potts, W., Madura, K., 1998. Rad23 links DNA repair to the ubiquitin/proteasome pathway. Nature 391, 715–718.

Schuberth, C., Buchberger, A., 2008. UBX domain proteins: major regulators of the AAA ATPase Cdc48/p97. Cell. Mol. Life Sci 65, 2360–2371.

Simpson, P.A., Spudich, J.A., Parham, P., 1984. Monoclonal antibodies prepared against Dictyostelium actin: characterization and interactions with actin. J. Cell Biol. 99, 287–295.

Song, C., Wang, Q., Li, C.C., 2003. ATPase activity of p97-valosin-containing protein (VCP). D2 mediates the major enzyme activity, and D1 contributes to the heat-induced activity. J. Biol. Chem. 278, 3648–3655.

Su, V., Lau, A.F., 2009. Ubiquitin-like and ubiquitin-associated domain proteins: significance in proteasomal degradation. Cell. Mol. Life Sci. 66, 2819–2833.

Tang, W.K., Xia, D., 2013. Altered intersubunit communication is the molecular basis for functional defects of pathogenic p97 mutants. J. Biol. Chem. 288, 36624–36635.

Wang, C.K., Broder, U., Weeratunga, S.K., Gasser, R.B., Loukas, A., Hofmann, A., 2012. SBAL: a practical tool to generate and edit structure-based amino acid sequence alignments. Bioinformatics 28, 1026–1027.

Watts, G.D., Wymer, J., Kovach, M.J., Mehta, S.G., Mumm, S., Darvish, D., Pestronk, A., Whyte, M.P., Kimonis, V.E., 2004. Inclusion body myopathy associated with Paget disease of bone and frontotemporal dementia is caused by mutant valosin-containing protein. Nat. Genet. 36, 377–381.

Weihl, C.C., Dalal, S., Pestronk, A., Hanson, P.I., 2006. Inclusion body myopathy-associated mutations in p97/VCP impair endoplasmic reticulum-associated degradation. Hum. Mol. Genet. 15, 189–199.

White, M.D., Ralston, G.B., 1976. A water-soluble Mg2+-ATPase from erythrocyte membranes. Biochim. Biophys. Acta 436, 567–576.

Wiesner, C., Faix, J., Himmel, M., Bentzien, F., Linder, S., 2010. KIF5B and KIF3A/KIF3B kinesins drive MT1-MMP surface exposure, CD44 shedding, and extracellular matrix degradation in primary macrophages. Blood 116, 1559–1569.

Williams, K.L., Newell, P.C., 1976. A genetic study of aggregation in the cellular slime mould *Dictyostelium discoideum* using complementation analysis. Genetics 82, 287–307.

Wittig, I., Schägger, H., 2008. Features and applications of blue-native and clear-native electrophoresis. Proteomics 8, 3974–3990.

Wittig, I., Karas, M., Schagger, H., 2007. High resolution clear native electrophoresis for in-gel functional assays and fluorescence studies of membrane protein complexes. Mol. Cell. Proteomics 6, 1215–1225.

Zerbetto, E., Vergani, L., Dabbeni-Sala, F., 1997. Quantification of muscle mitochondrial oxidative phosphorylation enzymes via histochemical staining of blue native polyacrylamide gels. Electrophoresis 18, 2059–2064.

Zhang, X., Shaw, A., Bates, P.A., Newman, R.H., Gowen, B., Orlova, E., Gorman, M.A., Kondo, H., Dokurno, P., Lally, J., Leonard, G., Meyer, H., van Heel, M., Freemont, P.S., 2000. Structure of the AAA ATPase p97. Mol. Cell 6, 1473–1484.

Zhang, X., Gui, L., Zhang, X., Bulfer, S.L., Sanghez, V., Wong, D.E., Lee, Y., Lehmann, L., Lee, J.S., Shih, P.Y., Lin, H.J., Iacovino, M., Weihl, C.C., Arkin, M.R., Wang, Y., Chou, T.F., 2015. Altered cofactor regulation with disease-associated p97/VCP mutations. Proc. Natl. Acad. Sci. U. S. A. 112, E1705–1714.